

Self-Similar Shocks in Polytopic Gas Flows around Star-Forming Regions

Yu-Qing Lou^{1,2,3,4} and Yang Gao¹

¹*Physics Department and Tsinghua Centre for Astrophysics (THCA), Tsinghua University, Beijing 100084, China; louyq@tsinghua.edu.cn; lou@oddjob.uchicago.edu; gaoyang-00@mails.tsinghua.edu.cn*

²*Centre de Physique des Particules de Marseille (CPPM)/Centre National de la Recherche Scientifique /Institut National de Physique Nucléaire et de Physique des Particules et Université de la Méditerranée Aix-Marseille II, 163, Avenue de Luminy Case 902 F-13288 Marseille, Cedex 09, France;*

³*Department of Astronomy and Astrophysics, The University of Chicago, 5640 South Ellis Avenue, Chicago, IL 60637 USA;*

⁴*National Astronomical Observatories of China, Chinese Academy of Sciences, A20, Datun Road, Beijing 100012, China.*

Accepted . Received ; in original form

ABSTRACT

Self-similar shock solutions in spherically symmetric polytopic gas flows are constructed and analyzed in contexts of proto-star formation processes. Among other possible solutions, we model a similarity shock across the sonic critical curve with an inner free-fall core collapse and a simultaneous outer expansion of the extended envelope; the separation or stagnation surface between these two flow zones travels outwards in a self-similar manner at a variable speed. One readily obtains accretion shock solutions. Semi-complete self-similar solutions across the sonic critical curve either once or twice without shocks can also be constructed. Features of star formation clouds of our polytopic model include the mass density scaling in the outer flow zone $\rho \propto r^{-2/(2-\gamma)}$, the temperature scalings of the inner flow zone $T \propto r^{-3(\gamma-1)/2}$ and of the outer flow zone $T \propto r^{-2(\gamma-1)/(2-\gamma)}$, and the variable central mass accretion rate $\dot{M} = k^{3/2} t^{(3-3\gamma)} m_0 / G$ where γ is the polytopic index, k is a constant, m_0 is the core mass, and G is the gravitational constant. Spectral line profiles characteristic of the ‘envelope expansion with core collapse’ (EECC) shock solutions are expected. Random magnetic field permeated in a partially ionized cloud can be incorporated into this theoretical polytopic model framework. We discuss briefly our results in context of the oft-observed starless B335 cloud system as an example.

Key words: ISM: H II regions — hydrodynamics — ISM: clouds — shock waves — stars: formation — stars: winds, outflows

1 INTRODUCTION

In astrophysical and cosmological contexts, the dynamic evolution of a spherical gas flow has been studied both numerically and analytically since late 1960s (Larson 1969; Penston 1969). Sufficiently far away from initial and boundary conditions, such flows may gradually evolve into a self-similar phase (Sedov 1959). Shu (1977) constructed the ‘expansion wave collapse solution’ (EWCS) in a self-gravitating isothermal gas cloud and advocated the so-called inside out collapse scenario for forming low-mass stars (Shu 1977; Shu, Adams & Lizano 1987). Such a similarity isothermal cloud collapse process involves a diverging mass density $\rho \propto r^{-3/2}$ and a diverging radial infall speed $v \propto -r^{-1/2}$ near the collapsing core yet with a $\rho \propto r^{-2}$ far away in a static envelope characterized

by the outer part of a singular isothermal sphere (SIS). The boundary of the infall region expands at a constant sound speed. For a more general polytopic gas, similarity solutions have also been derived and analyzed from various perspectives (Cheng 1978; Goldreich & Weber 1980; Yahil 1983; Suto & Silk 1988; McLaughlin & Pudritz 1997; Fatuzzo, Adams & Myers 2004; Lou & Wang 2006). With effects of unknown energetic processes relegated to the polytopic index γ , these polytopic solutions, among others, become more flexible and versatile in modelling core collapsing processes in a molecular cloud. Shocks can be constructed in an isothermal flow (Tsai & Hsu 1995; Shu et al. 2002; Shen & Lou 2004; Bian & Lou 2005; Yu, Lou, Bian & Wu 2006). These similarity shock solutions contain important realistic features to model large-scale flow dynamics around star-forming re-

gions. While there are two- or three-dimensional numerical simulations to model sub-structures in star-forming regions (Truelove et al. 1998), we explore in this paper the full extent of possible one-dimensional features under spherical symmetry that are extendable to two- or three-dimensional flow modelling in principle.

Recently, Lou & Shen (2004) obtained a novel class of semi-complete isothermal flows, including those referred to as ‘envelope expansions with core collapses’ (EECC) that may or may not involve the sonic critical line. Such solutions can model simultaneous inner collapse and outer flow expansion with or without shocks and are applied to star-formation regions such as B335 cloud system (Zhou et al. 1993; Shen & Lou 2004). In particular, Shen & Lou (2004) emphasized that a cloud envelope, with a central collapsing core to form a star or a star cluster, may either expand or contract depending on initial environmental conditions. Fatuzzo et al. (2004) considered a polytropic gas collapse under self-gravity in reference to observationally inferred far-away inflows. They adopted different polytropic indices for equations of state for an initial static cloud and a cloud in dynamic evolution in a more general manner. Central mass accretion rates are also examined as compared with observations (Fatuzzo et al. 2004). In this paper, we study polytropic gas flow solutions across the sonic critical curve either with or without shocks, which was not considered by Fatuzzo et al. (2004). Moreover, semi-complete EECC solutions crossing the sonic critical curve twice in a polytropic gas are also constructed as an extension of the isothermal result of Lou & Shen (2004). Both shock and EECC features are expected in clouds with collapsing cores surrounding proto-star forming regions. This theoretical development, together with shock modelling (Bian & Lou 2005; Yu & Lou 2005; Yu et al. 2006) and adaptations, may also bear physical implications for the dynamic evolution phase with a timescale of $\sim 10^3$ yrs linking AGBs and PNe (e.g., Balick & Frank 2002 and extensive references therein).

Observations of star-forming regions have been accumulating over years. Various optical, infrared, sub-millimeter and more recent X-ray observations reveal structures on different scales of hundreds of star-forming regions, a few of which are well observed (Zhou et al. 1993; Shirley & Evans II 2002; Swift et al. 2005) and become valuable sources for checking and testing theoretical model development. By simulating characteristic spectral line profiles given an underlying model of dynamic or magnetohydrodynamic (MHD) flows, one can infer information of a star-forming region by estimating the density and flow profiles, velocity dispersion, temperature scaling and central mass accretion rate and so forth.

With these considerations in mind, we present in §2 our polytropic similarity flow model, including the polytropic EECC and shock solutions. Several aspects of probing star-forming processes are discussed in §3. Further discussion of our model application is presented in §4. Several details of mathematical derivations are summarized in Appendices A, B and C for the convenience of reference.

2 SELF-SIMILAR POLYTROPIC GAS FLOWS

For the dynamical evolution of spherically symmetric gas flows under self-gravity and thermal pressure, we use the basic nonlinear fluid equations in spherical polar coordinates (r, θ, ϕ) , namely

$$\frac{\partial \rho}{\partial t} + \frac{1}{r^2} \frac{\partial}{\partial r} (r^2 \rho u) = 0, \quad (1)$$

$$\frac{\partial u}{\partial t} + u \frac{\partial u}{\partial r} = -\frac{1}{\rho} \frac{\partial p}{\partial r} - \frac{GM}{r^2}, \quad (2)$$

$$\frac{\partial M}{\partial t} + u \frac{\partial M}{\partial r} = 0, \quad \frac{\partial M}{\partial r} = 4\pi r^2 \rho. \quad (3)$$

Here mass density ρ , thermal gas pressure p and radial flow speed u are all functions of both radius r and time t , and equations (1) and (2) represent mass and momentum conservations, respectively; M is the total enclosed mass inside r at a given time t and the first of equation (3) is another form of mass conservation; the Poisson equation relating gas mass density and the gravitational potential is automatically satisfied and G is the universal gravitational constant.

The generalized polytropic relation takes the form of

$$p = K(t) \rho^\gamma, \quad (4)$$

where γ is the polytropic index and the coefficient $K(t)$ can vary with time t . The isothermal case corresponds to $\gamma = 1$ and a constant $K(t) = \kappa$. Equation of state (4) contains information of some unknown energetic processes. A time-dependent $K(t)$ leads to different solution families for $1 \lesssim \gamma \lesssim 2$, while for $p = \kappa \rho^\gamma$, the special cases of $\gamma = 4/3$ and $5/3$ should be handled separately (Cheng 1978; Goldreich & Weber 1980; Lou & Wang 2006).

We introduce the self-similarity transformation in the following form (Suto & Silk 1988; Lou & Wang 2006)

$$x = r/A(t), \quad M(r, t) = B(t)m(x), \quad u(r, t) = C(t)v(x),$$

$$\rho(r, t) = D(t)\alpha(x), \quad p(r, t) = E(t)\beta(x), \quad (5)$$

where the forms of functions $A(t)$, $B(t)$, $C(t)$, $D(t)$ and $E(t)$ should be properly chosen. Depending on x only, functions $\alpha(x)$, $v(x)$, $m(x)$ and $\beta(x)$ are the reduced density, radial velocity, enclosed mass, and thermal pressure, respectively. The scale-free independent variable x is defined following the power-law time dependence assumption $A(t) \propto t^n$ with n being a constant index; this self-similar independent variable is thus

$$x = r/(k^{1/2}t^n), \quad (6)$$

where k is a constant related to the polytropic sound speed $c \sim k^{1/2}t^{n-1}$. Here, the scale-free and self-similar independent variable x is made dimensionless and defined by $x = r/(ct)$, and the time variation of the polytropic sound speed c is related to the power-law time dependence $x = r/(k^{1/2}t^n)$.

By taking into account of the following scaling relationships $u \sim c$, $GM/r \sim u^2$, $M \sim \rho r^3$, $p \sim c^2 \rho$ and the equation of state (4), we can consistently cast the variables into the following form (see Appendix A for a more detailed

discussion)

$$\rho = \alpha(x)/(4\pi G t^2), \quad M = k^{3/2} t^{3n-2} m(x)/[(3n-2)G],$$

$$u = k^{1/2} t^{n-1} v(x), \quad p = k t^{2n-4} \alpha^\gamma(x)/(4\pi G), \quad (7)$$

where, in reference to equation of state (4), $K(t) \equiv k(4\pi G)^{\gamma-1} t^{2(\gamma+n-2)}$ is readily identified, and the polytropic sound speed defined by

$$c \equiv (\partial p / \partial \rho)^{1/2} = (k\gamma)^{1/2} t^{n-1} \alpha^{(\gamma-1)/2} \quad (8)$$

varies with t and r in general. By the definition of $K(t)$, $K(t) = \kappa$ becomes a constant coefficient for $n = 2 - \gamma$ and this corresponds to a conventional polytropic gas.

Introducing the self-similar transformation (7) to nonlinear partial differential equations (1), (2), (3), and (4), we readily obtain two coupled nonlinear self-similar ordinary differential equations (ODEs) (see Appendix B for a more detailed derivation), namely

$$[(v - nx)^2 - \gamma \alpha^{\gamma-1}](dv/dx) = (v - nx)^2 \alpha / (3n - 2) + 2(v - x) \gamma \alpha^{\gamma-1} / x - (v - nx)(n - 1)v \quad (9)$$

and

$$[(v - nx)^2 - \gamma \alpha^{\gamma-1}][d\alpha/(\alpha dx)] = (n - 1)v - (v - nx)\alpha / (3n - 2) - 2(v - x)(v - nx)/x. \quad (10)$$

In this procedure of derivation, an important result is $m(x) = \alpha x^2 (nx - v)$ (see equation B6), giving a clear physical requirement of $nx - v > 0$ for a positive enclosed mass. All the solutions seriously considered in this paper must satisfy this necessary requirement. By setting $v = 0$ for all $x > 0$, we obtain a static solution from equations (9) and (10), namely

$$v = 0, \quad \alpha = [2\gamma(3n - 2)/n^2]^{1/(2-\gamma)} x^{-2/(2-\gamma)},$$

$$m = (2\gamma)^{1/(2-\gamma)} (3n - 2)^{1/(2-\gamma)} n^{-\gamma/(2-\gamma)} x^{(4-3\gamma)/(2-\gamma)} \quad (11)$$

(Suto & Silk 1988; Fatuzzo et al. 2004), referred to as the singular polytropic sphere solution (Lou & Wang 2006).

We consider asymptotic solutions of equations (9) and (10) for $x \rightarrow 0^+$, $x \rightarrow +\infty$ and x near the sonic critical curve in the next subsection §2.1. Semi-complete solutions of the EECC type and shock solutions are constructed numerically in subsections §2.2 and §2.3.

2.1 Sonic Critical Curves and Asymptotic Behaviours of Self-Similar Solutions

Physically, when the travel speed of disturbances relative to the local flow speed is equal to the local sound speed, a singularity or a critical point arises. In steady flows of Bondi (1952) accretion and Parker (1958) solar wind, hydrodynamic solutions are obtained to go across the sonic critical point smoothly. Mathematically, we can construct the sonic critical curve by simultaneously setting the coefficients of dv/dx , of $d\alpha/dx$, and of the right-hand sides of equations (9) and (10) to vanish. The mathematical form of

the sonic critical curve is then specified by

$$nx_0 - v_0 = \sqrt{\gamma} \alpha_0^{(\gamma-1)/2},$$

$$(n - 1)v_0 + \frac{nx_0 - v_0}{(3n - 2)} \alpha_0 - 2 \frac{(x_0 - v_0)(nx_0 - v_0)}{x_0} = 0, \quad (12)$$

where the subscript 0 in variables x_0 , v_0 and α_0 indicates the explicit association with the sonic critical curve. The first equation in equation (12) is obtained from the coefficients of dv/dx and $d\alpha/dx$. The second equation in equation (12) can be obtained either from the right-hand side of equation (10) or from the right-hand side of equation (9), together with the first equation in equation (12). Several sonic critical curves of different parameters are shown in Figure 1 as examples of illustration.

To clarify solution behaviours near the sonic critical curve and to construct solutions across the sonic critical curve, we study asymptotic solutions (first-order Taylor expansion) of the form $x = x_0 + \delta$, $v = v_0 + v_1 \delta$ and $\alpha = \alpha_0 + \alpha_1 \delta$, where δ is a small displacement in x . By substituting these expressions into equations (9) and (10), the leading terms $\alpha_1 \equiv d\alpha/dx$ and $v_1 \equiv dv/dx$ satisfy the following two equations

$$\sqrt{\gamma} \alpha_0^{(\gamma-3)/2} \alpha_1 = v_1 - 2 + 2v_0/x_0,$$

$$(\gamma + 1)v_1^2 + [4(\gamma - 1)v_0/x_0 + n - 4\gamma + 1]v_1 + 2(2\gamma - 1)v_0^2/x_0^2 + 2[\alpha_0/(3n - 2) - 2n - 4\gamma + 4]v_0/x_0 + (n - 2)/(3n - 2)\alpha_0 + (2n + 4\gamma - 4) = 0, \quad (13)$$

respectively. Once parameters n and γ are specified and x_0 , v_0 and α_0 are determined from equation (12) for the sonic critical curve, $v_1 \equiv dv/dx$ can be solved from quadratic equation (13); $\alpha_1 \equiv d\alpha/dx$ can then be obtained from the first equation in equation (13) accordingly. These eigen-solutions in the vicinity of the sonic critical curve can be utilized to construct analytically smooth semi-complete solutions across the sonic critical curve without a shock. As the second equation in equation (13) is quadratic in v_1 , along certain segments of the critical curve, the eigensolutions may not exist. This situation does arise in constructing solutions shown in Figure 2.

To leading orders, asymptotic similarity solutions of coupled nonlinear ODEs (9) and (10) for $x \rightarrow +\infty$ and $x \rightarrow 0^+$ are summarized below. In the limit of $x \rightarrow +\infty$, we have

$$\alpha = A x^{-2/n}, \quad v = -\frac{nA}{(3n - 2)} x^{(n-2)/n} + \frac{2\gamma A^{\gamma-1}}{(2n + 2\gamma - 3)n} x^{(2-2\gamma-n)/n} + B x^{(n-1)/n}; \quad (14)$$

in the limit of $x \rightarrow 0^+$, the free-fall solution is

$$v = -\frac{(2m_0)^{1/2}}{x^{1/2}}, \quad \alpha = \frac{(3n - 2)}{2} \frac{(2m_0)^{1/2}}{x^{3/2}}, \quad m = m_0; \quad (15)$$

and in the limit of $x \rightarrow 0^+$, the polytropic counterpart of L-P type solution is

$$x \rightarrow 0^+ : \quad v = 2x/3, \quad \alpha = \alpha^*, \quad m = \alpha^* x^3 (n - 2/3), \quad (16)$$

where A , B , m_0 and α^* are relevant constants of integration.

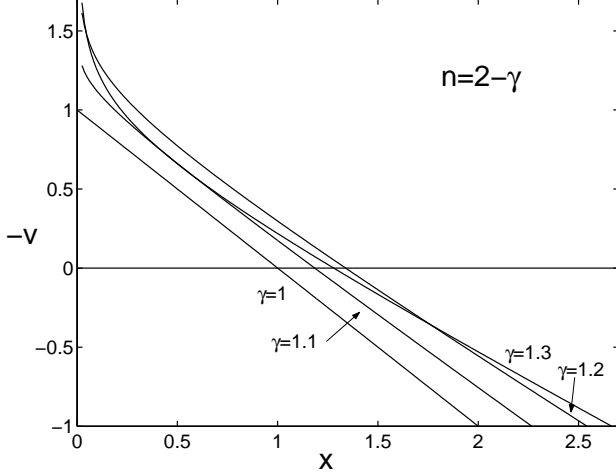


Figure 1. Sonic critical curves with $\gamma = 1, 1.1, 1.2$ and 1.3 in the case of $n = 2 - \gamma$ for a conventional polytropic gas. The sonic critical curves trace the locus of the sonic critical points $u = nr/t - c$. The sonic critical curve becomes a straight line only for $\gamma = 1$ corresponding to the isothermal case. With $\gamma = 1.1, 1.2$ and 1.3 , the sonic critical curves diverge for very small x .

These asymptotic solutions are found by comparing the leading terms of nonlinear ODEs (9) and (10) for $x \rightarrow +\infty$ and $x \rightarrow 0^+$, respectively. For $x \rightarrow 0^+$, two different solutions for the cloud with or without a central core m_0 are considered. If needed, higher-order expansion terms in these asymptotic solutions can be readily determined.

These leading scalings for $x \rightarrow 0^+$ [i.e., inner solutions for free falls (15) and expansions (16)] are independent of γ . For $x \rightarrow +\infty$, there is a constant speed solution for $n = 1$ corresponding to the isothermal case (Whitworth & Summers 1985; Lou & Shen 2004). For $x \rightarrow +\infty$ and $n = 2 - \gamma$, the gas flow Mach number $\mathcal{M} \equiv u/c$ remains constant as shown in equation (17) below.

$$\mathcal{M} \equiv \frac{u}{c} = \frac{v}{\gamma^{1/2} \alpha^{(\gamma-1)/2}} = \frac{Bx^{(n-1)/n} + \mathcal{O}[x^{(n-1)/n}]}{\gamma^{1/2} A^{(\gamma-1)/2} x^{(1-\gamma)/n}} = \frac{B}{\gamma^{1/2} A^{(\gamma-1)/2}} + \mathcal{O}(x^{-1/n}). \quad (17)$$

2.2 Polytropic EECC Similarity Solutions

We numerically solve coupled nonlinear ODEs (9) and (10) using available asymptotic solutions as ‘boundary conditions’. Eigensolutions near the sonic critical curve are determined by equation (13) in order to cross the sonic critical curve smoothly. However, for certain segments of the sonic critical curve, such eigensolutions of v_1 and α_1 do not exist. It is still possible to construct shock solutions across these sonic critical line segments (see §2.3).

It is simple to construct solutions not crossing the sonic critical curve by simply integrating from a chosen boundary condition. For solutions crossing the sonic critical curve smoothly, matching procedure of Lou & Shen (2004) is adopted for constructing semi-complete smooth solutions. That is, for the same solution, integrated results from the

inner and outer boundary conditions should match with each other at a chosen meeting point.

Displayed in Figure 2 are different types of flow solutions crossing or not acrossing the sonic critical curve. In this $-v$ versus x presentation, the first quadrant with $x > 0$ and $-v > 0$ physically represents collapse or inflow solutions, while the fourth quadrant with $x > 0$ and $-v < 0$ physically represents expansion, wind or outflow solutions. The solid curve spanning these two quadrants is the sonic critical curve as determined from equation (12). Three types of flow solutions are collapse/inflow solutions, envelope expansion with core collapse (EECC) solutions and L-P type solutions are shown together in Fig. 2.

These different kinds of dynamic solutions originate from different initial states, carrying sensible physical interpretations. Those curves diverging at small x have free-fall features, and the m_0 values marked along these curves represent their core masses. We observe that for a larger core mass m_0 , the outer part of the cloud tends to be an inflow. The solution curve marked with $m_0 = 3.20$ is connected to an outer initial state of $B = -0.1$, which represents an inflow (see equation 14 and note that in this $\gamma = 1.2$, $n = 1$ case, B is the leading term of $v_{+\infty}$). The flow curve with $m_0 = 1.77$ and $B = 0.1$ shows a breeze for $x > 17.5$, while the flow curve with $m_0 = 0.66$ and $B = 3.572$ shows an outflow at large x . On the other hand, both the inflow and outflow initial states at large x may involve an inner state without a central core (e.g., solution curves with $B = -1.797$ and $B = 2.230$ in Fig. 2). In short, we have the capability of constructing self-similar flow solutions passing through the sonic critical curve and making it possible to connect different inner and outer initial states in all feasible manner. Our polytropic model framework can accommodate various conditions for the inner and outer parts of a star-forming cloud.

Solutions spanning both the first and fourth quadrants represent the EECC feature. We see that both inner core collapse and outflow features exist in a semi-complete EECC similarity solution. This may be heuristically viewed as a combination of Bondi (1952) accretion and Parker (1958) solar wind such that the sonic critical curve are smoothly crossed twice (Lou & Shen 2004). We see also that a L-P type solution and an inner collapse solution with $m_0 = 0.40$ do not cross the sonic critical curve because of the absence of eigensolutions near the sonic critical curve (see equation 13 and the relevant discussion). Nevertheless, this problem can be solved by introducing a shock as shown in the next subsection. We focus on astrophysical applications of various EECC solutions in §3.

2.3 Various Similarity Shock Solutions

Shocks are introduced to match solutions from a given outer boundary condition and a certain solution from inner critical points or inner boundary conditions. For a polytropic gas, the shock jump conditions in the shock front reference

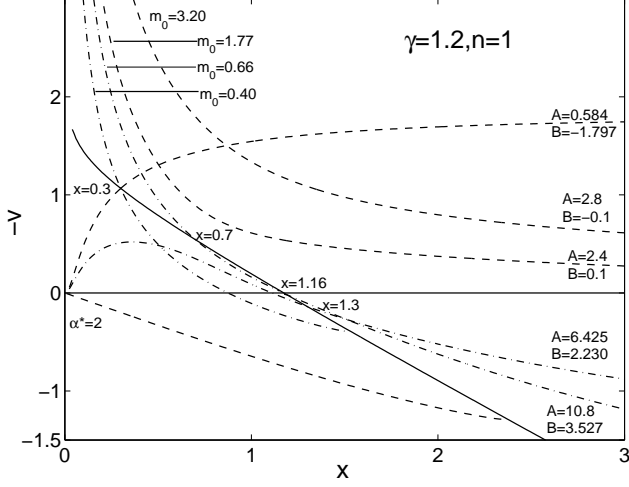


Figure 2. Three types of polytropic flow solutions for $\gamma = 1.2$ and $n = 1$ are constructed by specifying relevant parameters. The solid line is the sonic critical curve. Dashed curves in the first quadrant are collapse and inflow solutions. The incomplete dashed curve in the fourth quadrant which does not cross the sonic critical line is a counter part of the L-P solutions. The dash-dotted curves span two quadrants are EECC solutions.

framework are (Landau & Lifshitz 1959)

$$\rho_2/\rho_1 = \bar{u}_1/\bar{u}_2 = (\gamma + 1)\mathcal{M}_1^2/[(\gamma - 1)\mathcal{M}_1^2 + 2], \quad (18)$$

$$p_2/p_1 = 2\gamma\mathcal{M}_1^2/(\gamma + 1) - (\gamma - 1)/(\gamma + 1), \quad (19)$$

$$T_2/T_1 = [2\gamma\mathcal{M}_1^2 - (\gamma - 1)][(\gamma - 1)\mathcal{M}_1^2 + 2]/[(\gamma + 1)^2\mathcal{M}_1^2], \quad (20)$$

where \mathcal{M} is the flow Mach number in our reference framework, \bar{u} is the radial gas flow speed in the shock reference framework and subscripts 1 and 2 denote the pre-shock (upstream) and post-shock (downstream) sides of the shock, respectively. The ideal gas law is used here and T represents the gas temperature. These shock conditions are derived from the mass conservation, the momentum conservation and the formal entropy conservation along the streamline.

For gas flows with a constant polytropic index γ for the equation of state, the sound speed c jumps across the shock front because of the temperature discontinuity there. That is, $c_2/c_1 = (p_2/\rho_2)^{1/2}/(p_1/\rho_1)^{1/2} = (T_2/T_1)^{1/2}$, where c_1 and c_2 are pre-shock (upstream) and post-shock (downstream) sound speeds, respectively. Our definition of the self-similar independent variable x is of the scaling $x \sim r/(ct)$ (see equation 6 and the relevant discussion). Due to this jump in the sound speed c , independent variable x shifts in the self-similar framework accordingly across the shock front, namely

$$x_2/x_1 = (T_1/T_2)^{1/2}. \quad (21)$$

Therefore the same physical interface located at r at a given time t shows a separation across the shock front in our self-similar presentation because of this shock discontinuity shown in Figure 3.

From equations (7) and (18), we obtain the shock jump conditions in the shock reference framework in the reduced self-similar form

$$\alpha_2 = \frac{\alpha_1(\gamma + 1)(v_1 - nx_1)^2}{(\gamma - 1)(v_1 - nx_1)^2 + 2\gamma\alpha_1^{\gamma-1}}, \quad (22)$$

$$v_2 = nx_2 + \frac{x_2}{x_1(\gamma + 1)} \left[(\gamma - 1)(v_1 - nx_1) + \frac{2\gamma\alpha_1^{\gamma-1}}{v_1 - nx_1} \right] \quad (23)$$

(see Appendix C for details of derivation). Because of the entropy change across the shock front, the constant k is different on two sides of the shock front and the relation $(k_2/k_1)^{1/2} = x_1/x_2$ holds. We determine the post-shock quantities from the pre-shock physical conditions by applying equations (22) and (23). During this process of shock construction, equations (20) and (21) are used to determine the post-shock (downstream) independent variable x_2 . Thus these shock conditions serve as the condition to cross the sonic critical curve. Using the matching procedure of Shen & Lou (2004), we obtain different classes of shock solutions. That is, when integrated from an outer boundary condition to a certain place near the sonic critical curve, the jump conditions (22) and (23) are used to get the post-shock (downstream) quantities. Simultaneously, another asymptotic solution from an inner boundary condition is integrated outwards. When these two solutions match with each other in all quantities satisfying the shock conditions, a shock solution is then found.

Displayed in Figure 3 are different types of shock solutions with polytropic parameters $\gamma = 1.2$ and $n = 0.8$. In this presentation of $-v$ versus x , the first quadrant with $x > 0$ and $-v > 0$ physically represents collapse or inflow solutions. While the fourth quadrant with $x > 0$ and $-v < 0$ physically represents expansion, wind or outflow solutions. The solid curve spanning these two quadrants is the sonic critical curve. Dash-dotted straight lines connect the pre-shock and post-shock sides across the shock. These straight connection lines are not vertical because the same shock front has different scalings for the independent variable x on two sides in the self-similar framework (see equation 21). Three types of shock solutions are presented together, namely, shocks running into a static atmosphere, accretion shocks and wind shocks are shown in Figure 3.

We see that for the curve with the core mass parameter $m_0 = 1.51$, different kinds of shocks (shocks running into a static atmosphere and wind shocks etc.) can be constructed when the shock location or speed changes. Therefore the shock location is an additional parameter to join different inner (final) and outer (initial) conditions. For the same reason, shocks running into a static atmosphere (e.g., curves with $x_1 = 2.06$ and $x_1 = 4.4$) are constructed in both clouds with and without a central core.

From the two $B = -2$ and $B = 0.5$ curves in Figure 3, we note that an accretion shock can be constructed for a cloud either with or without a central core mass. A close look at the $B = 0.5$ curve shows that this is actually a ‘breeze’ shock solution which tends to be an outflow at a large x and the flow speed eventually approaches zero as $x \rightarrow +\infty$.

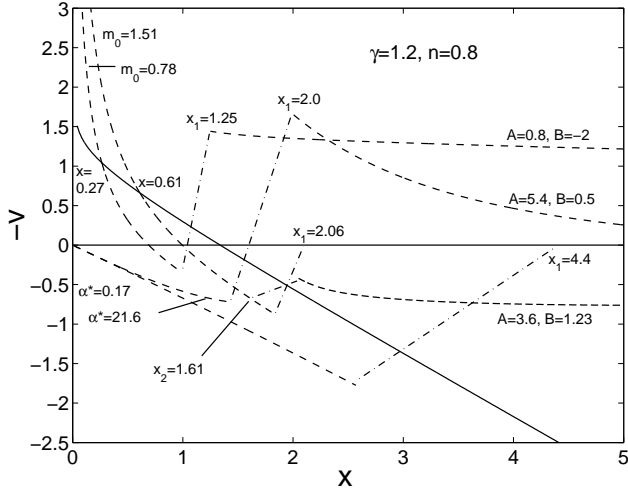


Figure 3. Three types of shock flows are constructed for $\gamma = 1.2$ and $n = 0.8$ with other parameters specified for a conventional polytropic gas. The solid line spanning the first and fourth quadrants is the sonic critical curve. Dash-dotted straight lines connect the pre-shock and post-shock sides (see equation 21 and the relevant discussion). The two dashed curves joining the $-v = 0$ axis at $x_1 = 2.06$ and $x_1 = 4.4$ are self-similar shocks running into a static atmosphere (i.e., the outer part of an singular polytropic sphere). The two curves with outer initial states characterized by $B = -2$ and $B = 0.5$ show shock discontinuities in the first quadrant; these are examples of accretion shocks. In contrast, the curve with $B = 1.23$ describes a wind shock.

(not shown in Fig. 3 because of scale restrictions). The pure coreless wind shock with $B = 1.23$ is a new addition to the shock solution family.

These shock solutions show various features for the inner and outer parts as in Fig. 2. The introduction of shocks enriches the variety of the semi-complete solution family (because shock location or speed itself is an additional parameter) and is qualitatively consistent with observations of star-forming regions (Nisini et al. 1999).

3 APPLICATIONS TO STAR-FORMING CLOUD CORES

There are several important observational aspects for an isolated star-forming region: the mass density profile, the temperature profile, the radial flow speed profile, the core mass accretion rate, magnetic field, and the angular momentum. In a spherically symmetric model, we consider and discuss the first five aspects except the last, and provide estimates of the star-forming cloud system B335.

Before coming to specific astrophysical applications, we clarify the physical meaning of similarity solutions passing through the sonic critical curve. For recent observations of star-forming regions, the features of inner part and outer edge are well observed and may serve as initial states for different kinds of star-formation models. Similarity solutions passing through the sonic critical curve with or without shocks can join all kinds of different inner and outer

physical states (see Figs. 2 and 3), while similarity solutions without crossing the sonic critical curve have much less freedom (Suto & Silk 1988; Fatuzzo et al. 2004). For example, the EECC solutions (Lou & Shen 2004), most of which pass through the sonic critical curve, represent a new class of similarity solutions that are not constructed previously without encountering the sonic critical curve. Polytropic shock solutions also form a new family; these shocks connect various inner and outer physical states and provide theoretical basis for modeling shock phenomena observed recently (Nisini et al. 1999).

3.1 Mass Density and Temperature Profiles in a Cloud with a Free-Fall Collapsing Core

By asymptotic solution (15) at small x , the inner collapsing core in a free-fall state of a pre-stellar region has a mass density profile of $\rho \propto r^{-3/2}$. This leading radial power-law scaling is also predicted by the isothermal model (Shu 1977; Lou & Shen 2004) and appears consistent with observations (Zhou et al. 1990; André et al. 2000). In other words, this information of inner mass density scaling alone cannot distinguish between polytropic and isothermal cloud models.

For the outer part of a pre-stellar region (sufficiently far away from the collapsing core), the isothermal cloud model gives a mass density profile $\rho \propto r^{-2}$, while the polytropic cloud model predicts $\rho \propto r^{-2/n}$ (see equation 14). Then for $n = 2 - \gamma$ corresponding to a constant $K(t) = \kappa$ in a conventional polytropic gas, the mass density profile for the outer part is

$$\rho \propto r^{-2/(2-\gamma)} \quad (24)$$

So $\gamma > 1$ means a density exponent smaller than -2 corresponding to a steeper density profile, while $\gamma < 1$ means a density exponent between -1 and -2 corresponding to a less steep density profile. Earlier observations gave a mass density profile with an exponent around -2 with considerable errors (Zhou et al. 1990). Recent observations show that this mass density exponent for the very outer parts (at radii $r \gtrsim 15,000\text{au}$) of starless cores is about -3 to -4 (André et al. 2000), corresponding to a polytropic index $\gamma \sim 1.3 - 1.5$. This observational evidence appears sensible and encouraging for a polytropic model.

Corresponding to the inner mass density profile $\rho \propto r^{-3/2}$, the radial scaling of thermal temperature T for an ideal gas in the inner free-fall region would be

$$T \propto p/\rho \propto r^{-3(\gamma-1)/2}. \quad (25)$$

This inner temperature T would be constant for an isothermal cloud model with $\gamma = 1$. The observed negative index of temperature scaling (Shirley & Evans II 2002) calls for $\gamma > 1$ in the inner region, qualitatively similar to the γ value inferred for the outer mass density profile. These radial scalings of cloud temperature are important features to constrain a polytropic cloud model by equations (24) and (25).

For the reference of observational diagnostics, the gas

temperature sufficiently far away (i.e., large r) from the collapsing core is given either by a constant T for an isothermal cloud model or by

$$T \propto p/\rho \propto r^{-2(\gamma-1)/(2-\gamma)} \quad (26)$$

for a conventional polytropic cloud model. Of course, the complete temperature profile in a conventional polytropic gas can be readily computed for observational comparison. The key message here is that independent determination of cloud temperature is extremely valuable for distinguishing models for cloud dynamics.

3.2 Radial Gas Flow Speed Profiles

Outflow features in star-forming regions are well documented in recent years. In spite of the large-scale bipolar morphology of these outflows, we are mainly interested in core regions of these outflow sources with free-fall collapse or infall characteristics (André et al. 2000; Wu et al. 2004; Swift et al. 2005) that are grossly in accord with our shock scenario of EECC.

Collapses and outflows were thought to happen in different stages during a star formation process, and they were considered separately (Shu 1977; Yahil 1983). However, at least $\sim 12\%$ of identified outflows show characteristics of collapses or infalls (Wu et al. 2004). Note that infall characteristics are more difficult to identify than those of an outflow due to the complexity of observed spectral lines and in the analysis of line profiles. One would expect that more infall motions can be identified in outflow sources in the future.

Our polytropic EECC shock solutions provide underlying dynamic models for simulating spectral line profiles, during a certain epoch of a star formation cloud. The most expected line profile features are those from EECC solutions, that is, inflow and outflow within and outside a certain radius r . Double peak spectral line features representing outflow will be observed away from the core, and combined double peak line features from both outflow and inflow will be seen around collapsing cores.

Using an isothermal model for self-similar cloud dynamics (Lou & Shen 2004), Shen & Lou (2004) emphasized the notion that a molecular cloud with a free-fall collapsing core at the centre can have various possible forms of motion sufficiently far away from the collapsing core, depending on the evolutionary history of the cloud. Such far away radial flows of a cloud may be characterized by a wind, a breeze, an outer part of a static singular isothermal sphere (SIS), a contraction, or an inflow. Furthermore, all these possible radial flow profiles can involve shocks across the sonic critical curve (Tsai & Hsu 1995; Shu et al. 2002; Shen & Lou 2004; Bian & Lou 2005). And this can give rise to a wide range for the central mass accretion rate to be discussed presently in the next subsection. All these important features in an isothermal cloud model can be further incorporated into a polytropic cloud model.

In reference to extensive cloud observations, Fatuzzo et

al. (2004) noted a ubiquitous feature of far away inflows and/or contractions in clouds with central free-fall collapsing cores. This differs from the static SIS envelope as initially introduced by Shu (1977) for the EWCS for star formation. The polytropic cloud model of Fatuzzo et al. (2004) also allows the polytropic indices to be different for an initially static cloud and for the subsequent evolution of a dynamic cloud. Nevertheless, Fatuzzo et al. (2004) did not consider self-similar polytropic flow solutions that cross the sonic critical curve smoothly and that involve shocks. Our model analysis here opens up these two important possibilities in a unified theoretical framework. Moreover, we emphasize again that in a polytropic cloud model, a cloud with a central free-fall core collapse can be simultaneously characterized by a far-away polytropic wind ($B \neq 0$ in equation 14) or a far-away polytropic breeze ($B = 0$ and $A \neq 0$ in equation 14) with or without shocks. Gas flows with central core collapse and far-away outflow or breeze are common in star-forming regions (Wu et al. 2004), indicating the capacity of our solutions passing through the sonic critical curve.

It is highly desirable to synthesize spectral line profiles using radial flow speed and mass density profiles from these underlying self-similar dynamic models for developing radiative diagnostics and for extensive observational comparisons.

3.3 Variable Central Mass Accretion Rate

The core mass accretion rate from equations (6), (7) and (15) is given by $\dot{M} = k^{3/2} t^{(3n-3)} m_0 / G$. For $n = 2 - \gamma$ corresponding to a constant $K(t) = \kappa$ of a conventional polytropic gas, the core mass accretion rate appears as

$$\dot{M} = k^{3/2} t^{(3-3\gamma)} m_0 / G \quad (27)$$

(see also equation 31 of Fatuzzo et al. 2004; the difference in a numerical factor is related to a different definition of notations), which is constant in the isothermal case of $\gamma = 1$ (Shu 1977). A constant \dot{M} is inconsistent with observations within a formation timescale of $\sim 10^5 - 10^6$ yr (André et al. 2000). The polytropic analysis does offer a possible leeway to model a variable \dot{M} in time t . For a fixed m_0 , there are two parameters k and γ to adjust. Here k is related to the sound speed c (see equation 6) and γ can be inferred observationally from the radial mass density profile as discussed in §3.1. For various shock solutions, the m_0 parameter can vary in a wide range. Although not easily done, it is crucial to identify the evolution phase of a dynamical cloud system and estimate or guess t accordingly as discussed presently.

For $\gamma < 1$ and $\gamma > 1$ in equation (27), the core mass accretion rate \dot{M} increases and decreases with time t , respectively. Observations of star-forming systems (André et al. 2000) indicate that mass accretion rates generally decrease in time t . This appears consistent qualitatively with $\gamma > 1$ for most cloud systems with free-fall collapsing cores. This inference of $\gamma > 1$ also agrees with the interpretation of steeper outer density profiles and the inner temperature power-law scaling with a negative index (see §3.1).

For shock flows, the core mass accretion rate varies with shock locations and thus shock speeds (Shen & Lou 2004; Bian & Lou 2005). This is because the value of m_0 is different for different shock locations.

The reason why $\gamma > 1$ or $\gamma < 1$ induce different \dot{M} is as follows. For $n = 2 - \gamma$ in equation (6), a physical interface for a fixed x travels with increasing speed for $\gamma < 1$. When this interface is set between the inflow and outflow regions at $v = 0$, we have an increase of infall mass $\dot{M} \propto \rho r^2 dr/dt$. For a fixed x , the product ρr^2 also increases with time t for $\gamma < 1$, then the increasing interface speed dr/dt leads to increasing mass infall rate. For $\gamma > 1$, the interface travels at a decreasing speed and the product ρr^2 also decreases, thus the mass infall rate decreases. When we set the interface at the shock location, the conclusion is that $\gamma < 1$ and $\gamma > 1$ lead to acceleration and deceleration of shocks, respectively.

3.4 Star-Forming Cloud System B335

The cloud system B335 is a well-studied protostellar collapse candidate that has been observed through molecular lines (Zhou et al. 1990; Harvey et al. 2003; Evans II et al. 2005). Data fitting and analysis of H_2CO and CS molecular transition lines agrees well with the inside-out collapse model (Shu 1977; Shu et al. 1987), yet the angular resolution of observations is still not good enough (Zhou et al. 1993). Recent observations of Institut de Radio Astronomie Millimétrique, Plateau de Bure Interferometer (IRAM PdBI) give several new results on this protostellar core (Harvey et al. 2003). First, a compact component with a circumstellar disc was identified. Secondly, the inner mass density profile is $\rho \propto r^{-p}$ with $p = 1.55 \pm 0.04$ in a certain region $r < R_0$. Thirdly, another valuable information is the gas temperature profile of $T \propto r^{-0.4}$ in a certain region $r < R_T$. Here, we tentatively take $R_0 \sim R_T \sim 5000\text{au}$.

The inner mass density profile $\rho \propto r^{-p}$ with $p = 1.55 \pm 0.04$ agrees with a free-fall core collapse ($p = 1.5$). Both polytropic and isothermal models show this scaling result. The outer density profile (3,500 – 25,000au) also shows a power law with an index $p = 1.91 \pm 0.07$. This result may be regarded as consistent with the isothermal model with $p = 2$, while the polytropic model can fit this result more accurately if we set $\gamma = 0.95$ in the outer part. One difficulty for the isothermal model is that the shallow slope ($p \sim 1$) of density profile at the edge of collapse region is still not observed (Harvey et al. 2003). But no shallow slope is necessary in the polytropic cloud model.

The temperature profile is $T \propto r^{-0.4}$ for $r < R_T = 5000\text{au}$, that is $T = 10\text{K}$ at $r > R_T$ and increase to $T \simeq 50\text{K}$ at $r \simeq 100\text{au}$ (Harvey et al. 2003). As observations show that $\rho \propto r^{-1.55}$ near the core, we need to set $\gamma = 1.26$ in the inner region to fit $T \propto r^{-0.4}$ (see equation 25). While one might use the isothermal model and assume different temperatures in different cloud regions, the polytropic cloud model with a temperature variation appears more sensible.

From the outer mass density profile and the inner temperature scaling of B335 system, we infer $\gamma = 0.95$ for

$3500\text{au} \lesssim r \lesssim 25,000\text{au}$ and $\gamma = 1.26$ for $r \lesssim 5000\text{au}$. This difference of γ shows that γ is not a constant at least for certain cloud systems with core collapses. Only when the outer mass density profile is steeper than $\rho \propto r^{-2}$, can γ become a constant.

Outflow and shock phenomena in B335 are also reported in recent years (Nisini et al. 1999). While previous isothermal solutions (Shu 1977) or polytropic solutions without crossing the sonic critical curve (Fatuzzo et al. 2004) cannot fit these observed conditions, these physical conditions can be related and constructed using an EECC shock curve passing through the sonic critical curve. Thus, this cloud system may be modelled as EECC self-similar shock solutions in a polytropic gas.

3.5 Magnetic Fields in Star-Forming Clouds

When a cloud is partially ionized, the magnetic field permeated in the cloud can exert an influence on the MHD evolution of the cloud system. Physically, magnetic field directly interacts with the charged particles which in turn interact with neutral particles through sufficiently frequent collisions. If the MHD timescale of interest is much longer than collision timescales between electrically charged and neutral particles, we may ignore the effect of ambipolar diffusion and adopt a MHD approximation to describe large-scale flows of a magnetized cloud. Moreover, the presence of magnetic field also leads to useful radiative diagnostics. For example, the presence of relativistic electrons produced by shocks or proto-stellar activities and of magnetic field together can give rise to cyclotron and synchrotron emissions.

Depending on the evolutionary history, magnetic field in a collapsing cloud under self-gravity may possess a variety of gross geometries (e.g., Chandrasekhar & Fermi 1953; Chandrasekhar 1954; Strittmatter 1966; Bisnovatyi-Kogan, Ruzmaikin, & Sunyaev 1973; Mestel 1986; Rees 1987; Lou 1996). We outline below a possible scenario involving magnetic field to pave the way for further investigations. It is perceived that a partially ionized gas cloud under self-gravity is permeated with a completely random magnetic field (e.g., Zel'dovich & Novikov 1971). For such a random magnetic field, we envision a random ‘thread ball’ scenario in a vast spatial volume of gas medium. A magnetic field line follows the ‘thread’ meandering within a thin spherical ‘layer’ in space in a random manner. Strictly speaking, there is always a random weak radial magnetic field component such that random magnetic field lines in adjacent ‘layers’ are actually connected throughout in space. By taking a large-scale ensemble average of such a magnetized gas cloud, we are then left with packed ‘layers’ of random magnetic field components dominantly transverse to the radial direction. Over large scales, the MHD collapse and flow in such a magnetized cloud are approximated as quasi-spherically symmetric (Yu & Lou 2006; Yu, Lou, Bian & Wu 2006; Wang & Lou 2006).

In addition to the thermal gas pressure force and self-gravity in the cloud, the magnetic Lorentz force consisting

of magnetic pressure and tension forces will come into play for a sufficiently strong magnetic field. MHD generalizations of isothermal hydrodynamic self-similar solutions are readily available (Yu et al. 2006). For example, for the MHD free-fall asymptotic solution towards the core, the magnetic field strength diverges yet the self-gravity remains overwhelming over the thermal pressure force and the Lorentz force combined. In such an MHD core collapse process, a strongly magnetized environment can be created and sustained surrounding a proto-stellar core. Accretion and rebound MHD shocks can emerge (Bian & Lou 2005; Yu et al. 2006; Wang & Lou 2006). Near the very centre, various magnetic activities, persistent or sporadic, are naturally expected to break the quasi-spherical symmetry as well as the self-similarity. If a cloud possesses an initial angular momentum, then such a core collapse under self-gravity will lead to a rapid gas rotation and a disc formation surrounding the proto-stellar core; in such a strongly magnetized environment, the coupling between the magnetic field and disc rotation can give rise to collimated outflows such as jets or winds (e.g., Lovelace 1976; Blandford & Payne 1982; Shu et al. 1997; Ferrari 1998). This type of MHD collapse processes may lead to intensely magnetized proto-stellar objects.

4 DISCUSSION

For star-forming cloud systems, the outer mass density profile, the inner and outer temperature profiles, and the core mass accretion rate are crucial to test or constrain a polytropic cloud model. Given a self-similar dynamic profile in a polytropic gas, spectral line profiles can be simulated. These spectral line profiles are very important to show different evolution epochs in forming proto-stars. In addition to forming proto-stars, the variable core mass accretion rate \dot{M} by equation (27) also bears physical implications for the dynamic evolution phase with a timescale of $\sim 10^3$ yrs linking AGBs and PNe (Balick & Frank 2002). Further observations and analysis are needed especially for post-PNe of different ages. We also expect adaptations of our polytropic shock model to a certain epoch of supernova explosions (Lou & Wang 2006), with radiation and neutrino pressures also taken into account.

Shock phenomena are common in forming proto-stars, formation and evolution of PNe, and supernova explosions; they are important for the gas heating, the production of high-energy photons, the synthesis of heavy elements, and the acceleration of cosmic ray particles. In these contexts as well as others, our polytropic shock model has wide applicability. Properties of polytropic shocks should be explored further to include radiation processes, magnetic field effects (Yu et al. 2006; Wang & Lou 2006) and atomic/nuclear processes associated with shocks.

Radiative transfer processes will be incorporated into our model to make the underlying dynamic processes ‘visible’. Spectral line profiles of certain atoms and molecules can reveal profiles of mass density, flow velocity and gas

temperature. The EECC profiles and shocks are the most important features. Certain spectral line features derived from various underlying dynamic solutions should be compared with observations. Recent and further high-resolution spectral IR and microwave telescopes will surely stimulate the development of dynamic study of star-formation, formation/evolution of PNe, SNe and other relevant astrophysical processes.

ACKNOWLEDGMENTS

This work was supported in part by the ASCI Center for Astrophysical Thermonuclear Flashes at the University of Chicago, by the Special Funds for Major State Basic Science Research Projects of China, by the Tsinghua Center for Astrophysics (THCA), by the Collaborative Research Fund from the National Science Foundation of China (NSFC) for Young Outstanding Overseas Chinese Scholars (NSFC 10028306) at the NAOC, CAS by the NSFC grants 10373009 and 10533020 at Tsinghua University, and by the Specialized Research Fund for the Doctoral Program of Higher Education 20050003088 and the Yangtze Endowment from the Ministry of Education at Tsinghua University. The hospitalities of the Mullard Space Science Laboratory of University College London, of Astronomy and Physics Department at University of St. Andrews, Scotland, United Kingdom, and of Centre de Physique des Particules de Marseille (CPPM/IN2P3/CNRS) et Université de la Méditerranée Aix-Marseille II, France are also gratefully acknowledged. Affiliated institutions of Y-QL share this contribution.

REFERENCES

- André P., 2000, in *Protostars and Planets IV*, ed. V. Mannings, A. P. Boss, S. S. Russell (Tucson: Univ. Arizona Press), 59
- Balick B., Frank A., 2002, *ARA&A*, 40, 439
- Barenblatt G. I., Guirguis R. H., Kamel M. M., Kuhl A. L., Oppenheim A. K., Zel’dovich Y. B., 1980, *J. Fluid Mech.*, 99, 841
- Bian F. Y., Lou Y.-Q., 2005, *MNRAS*, 363, 1315
- Bisnovatyi-Kogan G. S., Ruzmaikin A. A., Sunyaev R. A., 1973, *SvA*, 17, 137
- Blandford R. D., Payne D. G., 1982, *MNRAS*, 199, 883
- Bondi H., 1952, *MNRAS*, 112, 195
- Chandrasekhar S., Fermi E., 1953, *ApJ*, 118, 116
- Chandrasekhar S., 1954, *ApJ*, 119, 7
- Cheng A. F., 1978, *ApJ*, 221, 320
- Evans II N. J., Lee J.-E., Rawlings J. M. C., Choi M., 2005, *ApJ*, 626, 919
- Fatuzzo M., Adams F. C., Myers P. C., 2004, *ApJ*, 615, 813
- Ferrari A., 1998, *ARA&A*, 36, 539
- Goldreich P., Weber S. V., 1980, *ApJ*, 238, 991
- Harvey D. W. A., Wilner D. J., Myers P. C., *ApJ*, 596, 383
- Hunter C., 1977, *ApJ*, 218, 834
- Landau L. D., Lifshitz E. M., 1959, *Fluid Mechanics* (New York: Pergamon)
- Larson R. B., 1969, *MNRAS*, 145, 405
- Lou Y.-Q., 1996, *MNRAS*, 279, L67
- Lou Y.-Q., Shen Y., 2004, *MNRAS*, 348, 717

- Lou Y.-Q., Wang W. G., 2006, MNRAS, in press (astro-ph/0608043)
- Lovelace R. V. E., 1976, Nature, 262, 649
- McLaughlin D. E., Pudritz R. E., 1997, ApJ, 476, 750
- Mestel L., 1986, Phys. Scr., T11, 53
- Myers P. C., 2005, ApJ, 623, 280
- Nisini B., Benedettini M., Giannini T., Clegg P. E., di Giorgio A. M., Leeks S. J., Liseau R., Lorenzetti D., Molinari S., Saraceno P., Spinoglio L., Tommasi E., White G. J., Smith H. A., 1999, A&A, 343, 266
- Parker E. N., 1958, ApJ, 128, 664
- Penston M. V., 1969, MNRAS, 144, 425
- Rees M. J., 1987, QJRAS, 28, 197
- Sedov L. I., 1959, Similarity and Dimensional Methods in Mechanics (New York: Academic)
- Shen Y., Lou Y.-Q., 2004, ApJ, 611, L117
- Shen Y., Lou Y.-Q., 2006, MNRAS Lett., 370, L85 (astro-ph/0605505)
- Shirley Y. L., Evans II N. J., 2002, ApJ, 575, 337
- Shu F. H., 1977, ApJ, 214, 488
- Shu F. H., Adams F. C., Lizano S., 1987, ARA&A, 25, 23
- Shu F. H., Shang H., Glassgold A. E., Lee T., 1997, Sci, 277, 1475
- Shu F. H., Lizano S., Galli D., Cantó J., Laughlin G., 2002, ApJ, 580, 969
- Stanghellini, 2005, Invited review in the Proceedings of the ESO Workshop “Planetary Nebulae beyond the Milky Way”, Springer-Verlag
- Strittmatter P. A., 1966, MNRAS, 132, 359
- Suto Y., Silk J., 1988, ApJ, 326, 527
- Swift J. J., Welch W. J., Francesco J. D., 2005, ApJ, 620, 823
- Truelove J. K., Klein R. I., McKee C. F., Holliman J. H. II, Howell L. H., Greenough J. A., Woods D. T., 1998, ApJ, 495, 821
- Tsai J. C., Hsu J. J. L., 1995, ApJ, 448, 774
- Wang W. G., Lou Y.-Q., 2006, Phys. Rev. D, submitted
- Whitworth A., Summers D., 1985, MNRAS, 214, 1
- Wu Y., Wei Y., Zhao M., Shi Y., Qin S., Huang M., 2004, A&A, 426, 503
- Yahil A., 1983, ApJ, 265, 1047
- Yu C., Lou Y.-Q., 2005, MNRAS, 364, 1168
- Yu C., Lou Y.-Q., Bian F.Y., Wu Y., 2006, MNRAS, 370, 121 (astro-ph/0604261)
- Zel’dovich Ya. B., Novikov I. D., 1971, Stars and Relativity – Relativistic Astrophysics, Vol. 1, (The University of Chicago Press, Chicago)
- Zhou S., et al., 1990, ApJ, 363, 168
- Zhou S., Evans N. J., II, Kömpe C., Walmsley C. M., 1993, ApJ, 404, 232

APPENDIX A: DERIVATION OF SELF-SIMILAR TRANSFORMATION

We here provide a heuristic derivation of self-similar transformation (7). In the end, it is the self consistency counts.

The independent self-similar variable is [see eq. (6)]

$$x = r/(k^{1/2}t^n) \quad (\text{A1})$$

and thus the polytropic sound speed c scales as $\sim k^{1/2}t^{n-1}$. As the radial flow speed u and the polytropic sound speed c are expected to scale similarly, i.e., $u \sim c$, the radial flow speed takes the following form

$$u = C(t)v(x) = k^{1/2}t^{n-1}v(x). \quad (\text{A2})$$

From the scaling relationships $M \propto \rho r^3$ and $GM/\pi^2 \sim u^2/r$, we have ρ related to u and r in the form of $\rho \sim u^2/Gr^2$. In reference to equations (A1) and (A2), we then have the

mass density $\rho = v^2(x)/(Gt^2x^2)$. Therefore, we put the factor $1/x^2$ into the scale-free part and multiply a constant factor $1/(4\pi)$ for notational convenience and arrive at

$$\rho = D(t)\alpha(x) = \alpha(x)/(4\pi Gt^2). \quad (\text{A3})$$

There implies a relationship $\alpha(x) \propto v^2(x)/x^2$.

From the scaling relationship $M \sim \rho r^3$ and the two self-similar expressions (A1) and (A3), we have the enclosed mass M in the form of $M = k^{3/2}t^{3n-2}x^3\alpha(x)/4\pi G$. We then merge the factor x^3 into the scale-free part and multiply a numerical factor $4\pi/(3n-2)$ for notational convenience. It follows that the enclosed mass is in the form of

$$M = B(t)m(x) = k^{3/2}t^{3n-2}m(x)/[(3n-2)G]. \quad (\text{A4})$$

It is also apparent that the scaling $m(x) \sim x^3\alpha(x)$ holds.

The thermal gas pressure p has the scaling of $p \sim c^2\rho \sim kt^{2n-4}/(4\pi G)$, where the form of the polytropic sound speed $c \propto k^{1/2}t^{n-1}$ and equation (A3) are used. For the scale-free part, we refer to the equation of state (4) and obtain the relation $p = K(t)\rho^\gamma \sim \alpha^\gamma(x)$. Therefore, the thermal gas pressure takes the following form

$$p = E(t)\beta(x) = kt^{2n-4}\alpha^\gamma(x)/(4\pi G). \quad (\text{A5})$$

It immediately follows that $\beta(x) \sim \alpha^\gamma(x)$.

APPENDIX B: DERIVATION OF SELF-SIMILAR ORDINARY DIFFERENTIAL EQUATIONS

Here we provide the derivation of the two nonlinear coupled ODEs (9) and (10) using the self-similar transformation (7).

By the chain rule, the partial differentials of a general function $\mathcal{F}(r, t) = F(t)f(x)$ are:

$$\frac{\partial \mathcal{F}(r, t)}{\partial r} = F(t) \frac{df(x)}{dx} \frac{\partial x}{\partial r} = \frac{F(t)}{k^{1/2}t^n} \frac{df(x)}{dx}, \quad (\text{B1})$$

$$\begin{aligned} \frac{\partial \mathcal{F}(r, t)}{\partial t} &= \frac{dF(t)}{dt} f(x) + F(t) \frac{df(x)}{dx} \frac{\partial x}{\partial t} \\ &= \frac{dF(t)}{dt} f(x) - \frac{nrF(t)}{k^{1/2}t^{n+1}} \frac{df(x)}{dx}. \end{aligned} \quad (\text{B2})$$

Referring to these partial differentials and the self-similar transformation (7), equations (1), (2) and (3) can be readily reduced to

$$(v - nx) \frac{d\alpha}{dx} + \alpha \frac{dv}{dx} + \frac{2\alpha v}{x} - 2\alpha = 0, \quad (\text{B3})$$

$$(n-1)v + (v - nx) \frac{dv}{dx} + \gamma \alpha^{\gamma-2} \frac{d\alpha}{dx} + \frac{m}{(3n-2)x^2} = 0, \quad (\text{B4})$$

$$(3n-2)m = (nx - v) \frac{dm}{dx}, \quad \frac{dm}{dx} = (3n-2)x^2\alpha, \quad (\text{B5})$$

respectively. From equation (B5), it follows that

$$m(x) = \alpha x^2 (nx - v), \quad (\text{B6})$$

leading to a necessary physical requirement of $nx - v > 0$ for a positive enclosed mass; this is referred to in Section 2 of the main text.

Finally, from equations (B3), (B4) and (B6), we derive the two coupled nonlinear ODEs in terms of $v(x)$ and $\alpha(x)$

$$\begin{aligned} [(v - nx)^2 - \gamma\alpha^{\gamma-1}](dv/dx) &= (v - nx)^2\alpha/(3n - 2) \\ &+ 2(v - x)\gamma\alpha^{\gamma-1}/x - (v - nx)(n - 1)v \end{aligned} \quad (\text{B7})$$

and

$$\begin{aligned} [(v - nx)^2 - \gamma\alpha^{\gamma-1}][d\alpha/(\alpha dx)] &= (n - 1)v \\ &- (v - nx)\alpha/(3n - 2) - 2(v - x)(v - nx)/x. \end{aligned} \quad (\text{B8})$$

APPENDIX C: DERIVATION OF SHOCK CONDITIONS IN THE SELF-SIMILAR FRAMEWORK

We summarize here the derivation of shock conditions in the self-similar framework, namely, equations (22) and (23) in the main text.

In the reference framework of the shock front, the shock jump conditions for the mass density and flow velocity are shown in equation (18), where subscripts 1 and 2 denote the pre-shock (upstream) and post-shock (downstream) sides, respectively. Note that flow velocity in the reference framework of the shock front has the form of $\bar{u}_1 = u_1 - u_s$ and $\bar{u}_2 = u_2 - u_s$, where u_s is the radial travel speed of the shock front. The shock front can be identified with x_1 in the pre-shock (upstream) side. Thus referring to equation (6), the travel speed of a shock front is

$$u_s = dr/dt = d(x_1 k_1^{1/2} t^n)/dt = n k_1^{1/2} t^{n-1} x_1. \quad (\text{C1})$$

This travel speed of the shock front can be also derived from the post-shock (downstream) side, namely

$$u_s = dr/dt = d(x_2 k_2^{1/2} t^n)/dt = n k_2^{1/2} t^{n-1} x_2. \quad (\text{C2})$$

The shock front travel speed derived from the upstream and downstream sides should be the same. Thus, from expressions (C1) and (C2), we derive the discontinuity in constant k , namely

$$(k_2/k_1)^{1/2} = x_1/x_2. \quad (\text{C3})$$

This discontinuity in k originates physically from the discontinuity in temperature or entropy across the shock front, as discussed in Section 2.3 of the main text. We also list flow velocities in the shock reference framework here

$$\bar{u}_1 = u_1 - u_s = k_1^{1/2} t^{n-1} (v_1 - nx_1) \quad (\text{C4})$$

and

$$\bar{u}_2 = u_2 - u_s = k_2^{1/2} t^{n-1} (v_2 - nx_2). \quad (\text{C5})$$

Referring to the sound speed definition (8), the pre-shock (upstream) sound speed is $c_1 = \gamma^{1/2} k_1^{1/2} t^{n-1} \alpha_1^{(\gamma-1)/2}$. Then from equations (17) and (C4), the pre-shock (upstream) Mach number is

$$\bar{\mathcal{M}}_1 = \frac{\bar{u}_1}{c_1} = \frac{k_1^{1/2} t^{n-1} (v_1 - nx_1)}{k_1^{1/2} t^{n-1} \gamma^{1/2} \alpha_1^{(\gamma-1)/2}} = \frac{v_1 - nx_1}{\gamma^{1/2} \alpha_1^{(\gamma-1)/2}}, \quad (\text{C6})$$

where $\bar{\mathcal{M}}$ is the Mach number in the reference framework of the shock front. With this derived upstream Mach number,

we obtain from equations (7) and (18) the density discontinuity in the self-similar framework as

$$\alpha_2 = \frac{\alpha_1(\gamma + 1)(v_1 - nx_1)^2}{(\gamma - 1)(v_1 - nx_1)^2 + 2\gamma\alpha_1^{\gamma-1}}. \quad (\text{C7})$$

Finally from equations (18), (C3)–(C6), we derive the radial flow velocity discontinuity in the self-similar framework as

$$v_2 = nx_2 + \frac{x_2}{x_1(\gamma + 1)} \left[(\gamma - 1)(v_1 - nx_1) + \frac{2\gamma\alpha_1^{\gamma-1}}{v_1 - nx_1} \right]. \quad (\text{C8})$$